Adaptive Interference Cancellation System for Multi-hop Cellular Networks

Saad Mahboob, Shawn Stapleton and Sami Muhaidat

***Abstract*—Unwanted feedback between the donor (receive) and coverage (service) antennas of a relay (repeater) are created by the radio echoes from the local scatters and direct path antenna isolation limitations. These radio echoes create interference not only in the incoming signal from the base station, but also cause instability in the repeater. In this paper, we present an interference cancellation system (ICS) for the multi-hop cellular networks. We propose a novel multiple-tap radio echo suppressor to give better performance. Our proposed architecture requires few taps and the complexity is greatly reduced. Interference cancellation ability of the ICS is confirmed using a test bench realized on a Xilinx Virtex-4 FPGA platform.**

***Index Terms*— Relay, ICS, coupling, FPGA**

I. Introduction

A. Background

THE Next generation wireless networks will support high data rates up to 100 Mbit/s for high mobility users and approximately 1 Gbit/s for low mobility users. Under certain conditions, e.g., limited frequency resources and blind spots in the existing cellular networks, the conventional approach is to increase the density of base stations (BSs), which is inefficient due to the high deployment cost. An alternative solution is to integrate the so-called multi-hop relaying (cf. Fig. 1), which has been traditionally studied in the context of ad-hoc and peer-to-peer network, into cellular wireless networks [1].

In multi-hop relaying, information is communicated between the two terminals (nodes) over multi-hop transmission. The multi-hop approach realizes several key advantages as compared to single hop scenario, e.g., lower power consumption and better throughput.

Traditionally, half duplex relay nodes are assumed in multi-hop networks. However, a recent trend among the relay designers is to use the term on-frequency (or single frequency network repeater (SFN)) repeaters, i.e., sending and receiving simultaneously in the same frequency band. Repeaters consist of two antennas, a receiver and a power amplifier. The antennas are identified as donor (receive) and coverage (service) antennas. The two antennas are typically mounted on the same tower and are located in close proximity. Since the single frequency network (SFN) can save frequency resources with a reasonable cost, the SFN repeater is a good solution for extending the coverage area [2], [3], [4].

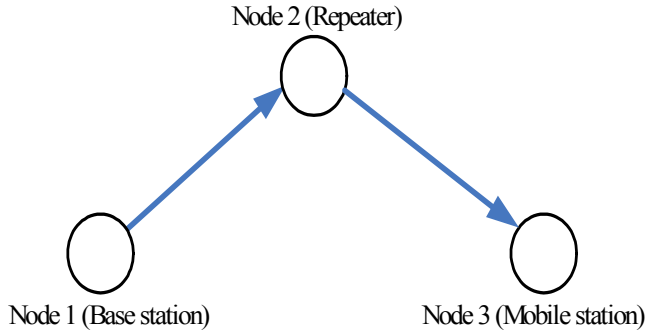

Fig. 1. Multi-hop wireless network.

Typically, repeaters are being used in environments where there is a physical separation between the two antennas, thereby reducing unwanted mutual coupling effects. However, in some scenarios, a physical separation between the antennas may not be possible, e.g., when deploying a repeater in a rural coverage, where both antennas are located at the same site (or even on the same post). As a result, radio echoes are generated between the donor and coverage antennas. As with any system with a feedback, this could cause the repeater to become unstable. Specifically, these radio echoes cause the relay to oscillate, thus, becoming unstable. Therefore, in order to reduce the effect of mutual coupling, antennas of the repeater are spatially separated or the gain of the repeater is decreased [4], [5], [6], [7]. These problems make the repeater restrict its transmission power, resulting in shrinkage of the coverage area. To gain additional isolation, various adaptive feedback cancellers have been discussed in the literature [2]-[12]. A frequency domain adaptive interference suppression algorithm is presented in [8], whereas [2], [5] and [6] present time domain least mean square (LMS) adaptive algorithms. Similarly, [9] presented an ICS for a CDMA network with a reduced processing delay, and fewer filter taps.

B. Contribution of this Paper

Unlike published works, this paper presents an ICS scheme for multi-hop WCMDA 3G networks. WCDMA is a leading

Manuscript received November 30, 2010.

Saad Mahboob was with Simon Fraser University, Burnaby, V5A1S6 Canada. He is now with the Department of Electrical and Computer Engineering, University of British Columbia, Vancouver, Canada (e-mail: smahboob@interchange.ubc.ca).

Shawn Stapleton and Sami Muhaidat are with Simon Fraser University, Burnaby, V5A1S6, Canada. (e-mail: shawn@sfu.ca, hma33@sfu.ca).

choice of data communication in the wireless industry nowadays and has been selected as an air interface for the third generation mobile communications. WCDMA supports a higher data rate then CDMA and is less susceptible to narrowband interferers and multipath fading.

This paper presents a novel multi-tap radio echo suppressor (RES) for the ICS. This novel architecture has the ability to reduce the estimation error if the echo-searcher gives an incorrect estimate of the position of the dominant echoes in the power delay profile (PDP).This is significant, since, the adaptive algorithm stability and convergence depends upon the precision of the calculated delay of the radio echoes. Our RES requires very less number of taps as compared to the other adaptive approaches, to cancel the feedback interference. Hence the implementation complexity is significantly reduced.

We further develop the interference cancellation system using a Xilinx XtremeDSP Development Kit using a Virtex-4 FPGA. This paper also simulates different properties of the ICS relay, including its tracking performance and phase cancellation ability. The effect of SNR, radio echo Doppler frequency and step-size factor on the tracking performance of ICS are also examined via simulation. The performance of the relay is further evaluated using a suppression measurement technique calculated using the frequency domain spectra and error vector magnitude (EVM).

The paper is organized as follows. The channel model is introduced in Section II. The system architecture is briefly presented in Section III. The multiple-tap radio echo suppressor (RES) architecture is presented in Section IV. The configuration of the ICS is discussed in Section V. Simulation results are discussed in Section VI. The FPGA measurement results are presented in Section VII. Finally, the paper is concluded in Section VIII.

II. Channel Model

The channel between the donor and coverage antennas of a repeater is modeled as a frequency selective Rayleigh fading channel. It can be represented by the following complex valued low-pass impulse response,

$$h(t) = \sum_{b=1}^{P-1} a_b(t) e^{-j\theta_b(t)} \delta(t - \tau_b) \tag{1}$$

where $\delta(\cdot)$ is the Dirac delta function, b is the channel index, P is the total number of multipath channel components, $a_b(t)e^{-j\theta_b(t)}$ are the time dependent channel coefficients which are usually complex Gaussian distributed and τ_b is the delay between the first tap and the b^{th} tap. The channel coefficients are independent and identically distributed. Typically, the channel taps decay according to an exponential profile. The amplitudes $a_b(t)$ follow a Rayleigh distribution whereas the phases $\theta_b(t)$ follow a uniform distribution. The channel between the repeater antennas is assumed to be very slowly varying. This implies that the path gains change insignificantly over a period of $1/F_D$, where F_D corresponds to maximum radio echo Doppler frequency. Mean Square Error (MSE) is used as a performance criterion to calculate the error between the ideal channel gain and estimated one. MSE is defined as follows,

$$MSE = \mathbf{E}\left(|w_l + M_l|^2\right) \tag{2}$$

i.e., ensemble average of squared absolute error between the ideal and estimated channel gains, where w_l and M_l are the ideal and estimated channel gains respectively and $\mathbf{E}(\cdot)$ is the ensemble average operator. w_l and M_l are complex quantities having a certain magnitude and phase. l is used as an iteration index. The ensemble average is usually calculated by averaging the MSE over a number of independent trials. The relay feedback channel impulse response normally consists of one or few large static feedback paths and a number of small Doppler feedback paths. Fig. 2 shows an example of the channel impulse response. In Fig. 2, the echoes at 0.01 μs and 1 μs have the dominant contribution in the channel impulse response, and have static positions. These echoes may be caused by the nearby static building and reflectors. The echoes at 3 μs and 5 μs can be considered as reflections from moving objects like cars and other vehicles; and may have an offset from their current positions in the delay profile.

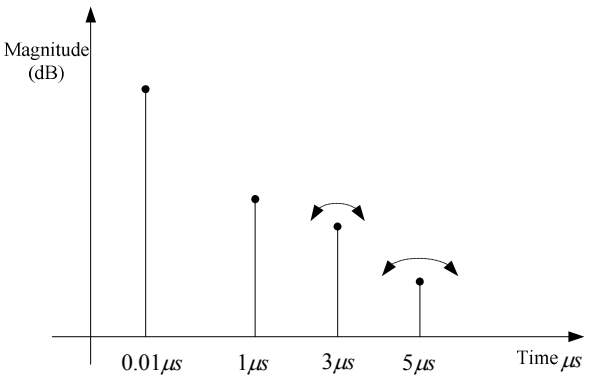

Fig. 2. Feedback coupling channel impulse response.

III. RES Architecture

A. ICS System

The proposed ICS requires adaptive filter taps exactly equal to the length of the channel impulse response. As an example, 4 taps are required for the impulse response in Fig 2. This reduces the complexity in comparison to other adaptive filter approaches. The path between antennas of a repeater includes a receiver, a de-correlation delay τ and a power amplifier. The delay τ is used to ensure that the signals coming from the BS are uncorrelated with the feedback radio echoes. The signal $C(n)$ at output of the repeater is delayed to match the delay of the echo $U_a(t)$, where the subscript a denotes the analog nature of the signal. The echo delay D is calculated in the relay by the echo searcher module. Correlation is used in the radio echo searcher (RES) to generate the normalized

correlation error signal Λ_l. A step-size μ is multiplied with Λ_l and this weighted signal is multiplexed with the delayed version of the signal $C(n)$ to generate the suppression signal $S(n)$. The suppression signal is then added to the incoming signal $R(n)$ to cancel the interference.

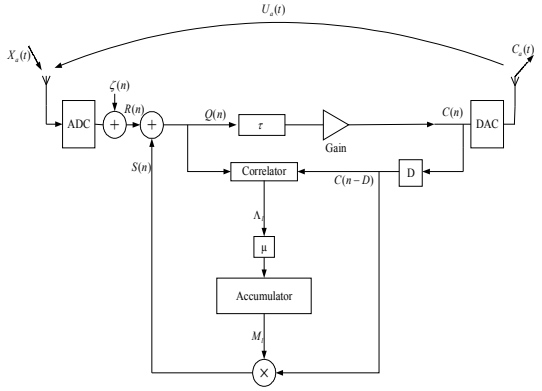

Fig. 3. Block diagram of single-tap RES.

Fig. 3 shows the block diagram of the RES. For simplification, we assume that the gain of the repeater is unity. Transmitted signal from the base station $X_a(t)$ and coupling signal $U_a(t)$ are received at the donor antenna and translated to baseband as,

$$R(n) = X(n) + U(n) \tag{3}$$

$U(n)$ and $X(n)$ are discrete-time counterparts of $U_a(t)$ and $X_a(t)$ respectively. Radio echo $U(n)$ is a delayed and attenuated version of the output signal $C(n)$. The de-correlation delay τ is chosen to be much greater than the symbol period T_{symbol} i.e. $\tau >> T_{symbol}$, to insure that the signals $X(n)$ and $C(n)$ are uncorrelated with each other. τ is defined as,

$$\tau = N_o T_s \tag{4}$$

where N_o is an integer number of samples. When the suppression signal $S(n)$ is added to the received signal $R(n)$ (containing the interference), the residual component (system error) $\varepsilon_{system}(n)$ is generated.

$$\varepsilon_{system}(n) = U(n) + S(n) \tag{5}$$

$\varepsilon_{system}(n)$ is useful to calculate the system mean square error MSE_{system}. MSE_{system} is closely related to MSE as derived in Appendix I. Equation (5) can be expressed as (see Appendix II),

$$\varepsilon_{system}(n) = C(n-D) \times e^{j\phi_{w_l}} \left(|w_l| - |M_l| \right) \tag{6}$$

where $|w_l|$ and ϕ_{w_l} represent magnitude and phase components of the complex channel gain w_l; and $|M_l|$ represents the magnitude of the estimated channel gain. After the signals $S(n)$ and $R(n)$ are added together, the resultant signal used as input to the correlator is [9],

$$Q(n) = R(n) + S(n) \tag{7}$$
$$= X(n) + \varepsilon_{system}(n) \tag{8}$$

B. Cost Function Formulation

As the interference signal $U(n)$ is cancelled by the suppression signal $S(n)$, the power of the residual signal $\varepsilon_{system}(n)$ decreases. In this work, average energy of the signal $Q(n)$ is taken as a cost function J.

$$J_l = \mathbf{E}\left(|Q(n)|^2 \right) \tag{9}$$

(9) can be simplified to (detailed proof in Appendix III),

$$J_l = \sigma_X^2 + |w_l + M_l|^2 \sigma_C^2 + 2|w_l + M_l| \Re[\psi] + \sigma_\zeta^2 \tag{10}$$

where ζ is the noise term modeled as zero mean Gaussian, $\Re[\psi]$ is the complex correlation operation between the signals $X(n)$ and $C(n-D)$ and is a negligible quantity, because of the chosen delay τ. The signals $X(n)$ and $C(n-D)$ are assumed to be independent of ζ. σ_X^2 denotes the variance of the signal coming from base station $X(n)$, σ_C^2 denotes the variance of the signal $C(n)$ and σ_ζ^2 represents variance of the noise ζ. Finally,

$$J_l = \sigma_X^2 + \sigma_\zeta^2 + |w_l + M_l|^2 \sigma_C^2 \tag{11}$$

Equation (11) plotted in Fig. 4 shows that cost function has an optimum value w_o when,

$$M_l \approx -w_o \text{ as } l \to \infty \tag{12}$$

This implies that cancellation of the radio echo is achieved by generating a suppression coefficient M_l which has the same magnitude but opposite phase to that of channel gain w_l. The resulting minimum mean square error (MMSE) is,

$$J_{\min} = \text{MMSE} = \sigma_X^2 + \sigma_\zeta^2 \tag{13}$$

This result shows that MMSE depends upon the variance of the transmitted signal from the BS and variance of the noise.

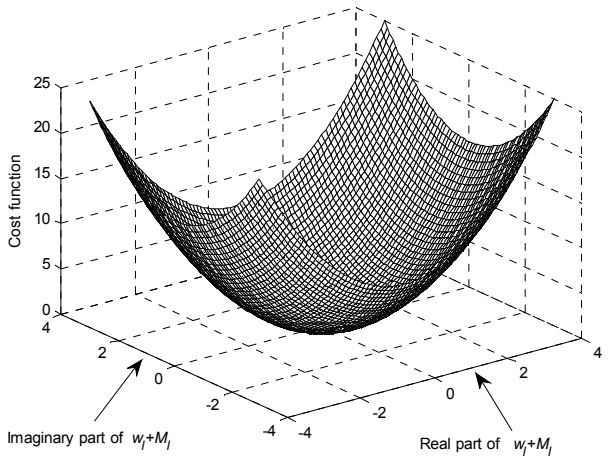

Fig. 4. Cost function of single-tap RES.

C. Steepest Descent Algorithm

Steepest descent algorithm (SDA), also called gradient descent algorithm, is an iterative technique used to approximate the optimum value of the cost function. To calculate the optimum point, the steepest descent algorithm takes steps proportional to negative of the gradient of the cost function at the current point. Given the cost function J and without any knowledge about its minimum value, the aim is to find a recursive procedure that starts with an initial guess for M_l, and then improves the guess in a recursive manner until the optimum value $M_l = -w_o$ is reached. The procedure that SDA follows is of the form,

new estimate = old estimate + correction term

or more explicitly,

$$M_l = M_{l-1} + \mu \times \rho\,, \qquad l \geq 1 \tag{14}$$

In (14), M_{l-1} is the channel gain estimate at iteration $(l-1)$ and M_l is the updated channel gain estimate at iteration l. The correction term is a product of a scalar μ and factor ρ. ρ is a function of some error i.e., $\rho = f(error)$ where $f(\cdot)$ denotes the function. The product $\mu \times \rho$ then defines the direction in which the current estimate is to be corrected for guaranteed convergence. The step-size μ determines how small or large the correction term will be and is a negative constant. μ and ρ are selected to enforce the condition $J(M_l) < J(M_{l-1})$. In this way, the value of the cost function in successive iterations will be monotonically decreasing until the estimate reaches the optimum value.

D. Adaptive Algorithm

The cancellation signal is generated using the signal,

$$C(n) = X(n-\tau) + \varepsilon_{system}(n-\tau) \tag{15}$$

This signal is passed through the delay D to get,

$$C(n-D) = X(n-\tau-D) + \varepsilon_{system}(n-\tau-D) \tag{16}$$

In an ICS relay, the complex signal samples $Q(n)$ and $C(n-D)$ given by (8) and (16) respectively, are correlated to produce the correlation error signal $e_l(n)$.

$$e_l(n) = Q(n) \times C(n-D)^* \tag{17}$$

$$= \left[X(n) + \varepsilon_{system}(n) \right] \times \left[X(n-\tau-D) + \varepsilon_{system}(n-\tau-D) \right]^* \tag{18}$$

Because of the de-correlation delay τ, the correlation between the signals $X(n)$ and $X(n-\tau-D)^*$ is very small and can be ignored. Likewise, $\varepsilon_{system}(n)$ can be expressed as a function of the signal $X(n)$ and hence the correlation between $\varepsilon_{system}(n)$ and $X(n-\tau-D)^*$ is negligible. Finally, (18) can be reduced to,

$$e_l(n) = \varepsilon_{system}(n) \times \varepsilon_{system}(n-\tau-D)^* \tag{19}$$

Thus, $e_l(n)$ depends upon correlation of the residual terms. (19) is integrated over the correlation period N to get the accumulated error signal E_l.

$$E_l = \sum_{i=0}^{N} e_l(i) \tag{20}$$

The accumulated error E_l is used in the SDA to update the channel gain estimate. Usually, normalized correlation error Λ_l is used since the accumulated error E_l given by (20) can yield a large number. Normalization on the other hand gives a relative value; that varies between $+1$ and -1.

$$\Lambda_l = \frac{E_l}{\sqrt{\sum_{i=0}^{N} |Q(i)|^2 \times \sum_{i=0}^{N} |C(i-D)|^2}} \tag{21}$$

Λ_l is used as an error function in the SDA, i.e.

$$\rho = \Lambda_l \tag{22}$$

Equation (14) then becomes,

$$M_l = M_{l-1} + \mu \times \Lambda_{l-1} \tag{23}$$

Step-size μ is chosen as a compromise between the speed of convergence and SNR. In practice, a large value of the step-size yields fast convergence that allows the algorithm to track rapid fluctuations due to fading, at the expense of increased noise in the channel gain estimate which affects the interference cancellation. Similarly, a small value of the step-

size makes convergence of the adaptive algorithm slow.

IV. A Novel Multiple-tap RES Architecture

In section III, we have assumed that the echo-searcher provides the exact delay D of the radio echo. We have overlooked the scenario where the delay D is incorrectly detected, which could result in performance degradation. In this situation, the RES will not effectively suppress the interference radio echo. To solve this issue, we propose a novel multiple-tap RES architecture. The multiple-tap RES has the ability to give acceptable interference cancellation results (not the optimum) even when the correct value of the echo delay D is unavailable. This is accomplished by making use of a delay-line i.e. $D+1$, D and $D-1$ in the RES instead of a single delay D. Thus for example, if the exact position the echo is at 100th time index; and the echo-searcher mistakenly gives the echo delay of 101, the multiple-tap RES makes use of delays 101,100 and 99 in its architecture. The echo values at 99th and 100th time-index may be considered as a source of an additional noise to the adaptation process. Interpolation can be used to increase the accuracy of the echo delays. Fig. 5 shows the block diagram of multiple-tap RES. The Fig. 5 shows three correlators in the architecture. In reality, we can use the result of only correlator to get the errors for all the three adaptive filters. As shown later in the simulation results, using a multiple-tap RES has an advantage of reduced MSE, in the presence of echo-delay estimation error, but at the expense of a slight increase in the RES architecture complexity.

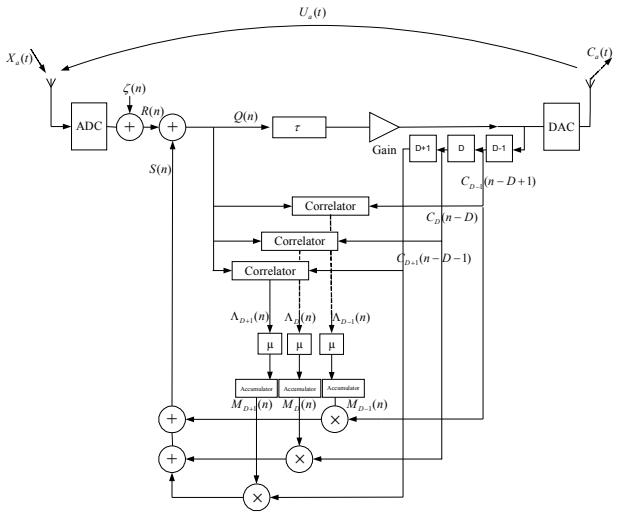

Fig. 5. Block diagram of multiple-tap RES.

V. Configuration of ICS

Since RES is capable of tracking a single radio echo, so in order to suppress several radio echoes simultaneously, several RESs are to be programmed on the FPGA and arranged in parallel. Such an alignment of the RESs is termed as multiple radio echo suppressor (MRES). In addition, an echo-searcher is also programmed on the same chip. The radio echo-searcher works at a much lower clock rate than the MRES. If a new echo is detected, the echo searcher informs the controller to take a desired action. Usually, radio echo suppressors are used successively, starting from echo with the biggest magnitude in the power delay profile (PDP). If the echo-searcher finds a new radio echo, the controller assigns an unused RES to it for suppression. Similarly, the echo suppressor is set to an idle state when its contribution in the overall interference cancellation is small. The contribution of active echo suppressors, in the overall interference cancellation, is periodically monitored by the controller, by observing the output of the correlator in each RES. Fig. 6 shows the block diagram of a complete ICS.

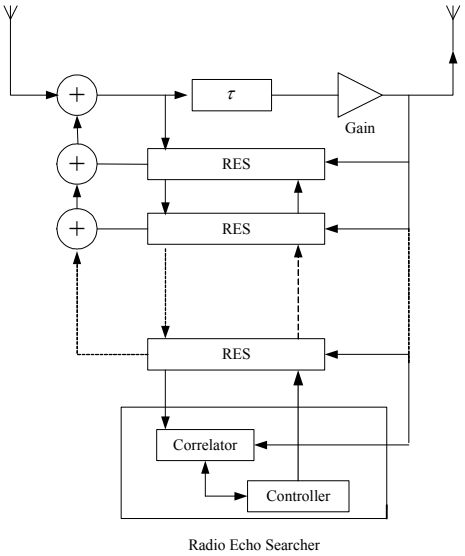

Fig. 6. Complete ICS with MRES and a radio echo searcher.

VI. Simulation Results

In this section, we illustrate different features of the Multi-hop ICS repeater. An ICS with three echo suppressors is implemented. In this paper, we assume frequency selective Rayleigh fading channels. In the frequency selective channel, the signal is received due to multiple versions of the transmitted signal, attenuated and delayed in time due to the radio echoes. The variance of the BS transmitted signal is set to 1 watt and radio echo Doppler frequency is assumed to be 10 Hz. The mean values of the three echoes are 0.4, 0.3 and 0.2, which correspond to echoes with -8 dB, -10 dB and -14 dB less power respectively, than the power of transmitted signal from BS. The value of the step-size μ is set to 0.0001.

Fig. 7 shows the three feedback cancellers in the ICS relay tracking the magnitude components of the respective echoes. It is clear from Fig. 7 that the ICS works quite well in deep fading environment. The three suppressors work independently because of the in-built correlation property of the WCDMA signal. The system can best track the feedback echo if the echo level is above the threshold value. As the power level of the echo in the delay profile decreases, the RES finds it difficult to track the time-varying radio channel, due to the presence of the system noise-floor. This makes the adaptive filter difficult to track the fading channel.

The phase cancellation ability of the radio echo suppressors

is simulated in Fig. 8. For every radio echo suppressor, the suppression coefficient M_l has an angle π radian out of phase to the angle of w_l. The phase plots in Fig. 8 are shown as unwrapped. The phases of the suppression signal and interference coupling signal are added together to give a straight line representing either π or $-\pi$ radians.

The interference cancellation ability of ICS relay is preferably calculated using the spectral plots. The measuring index of the interference cancellation performance is decibel cancellation (dBc) relative to the interference signal. Fig. 9(a) shows the spectrum of the interference coupling signal. The average power spectral density (PSD) of the coupling signal is 10 dB less than the average PSD of transmitted signal. Fig. 9(b) shows the spectrum of the output re-transmitted signal, when the ICS is active. Table. I gives the averaged spectrum values of various signals. In Table. I, the dBc is determined by taking the absolute value of the difference between the average value of the interference signal and the average value of the error signal.

Error vector magnitude (EVM) is a measure used to quantify the performance of the digital receiver (in this case, ICS). Informally, EVM is a measure of how far the received symbols are away from their ideal locations in the constellation plot. In our simulations, WCDMA signal is transmitted from the BS and corrupted by the AWGN noise. The SNR of this signal is 25 dB and its EVM is 7.6%. Fig. 10(a) shows the constellation of the signal at the output of the ICS, when it is turned off. The EVM of this signal is 36.67%. The constellation of the output signal, when the ICS is active is shown in Fig. 10(b) and its EVM is calculated to be 10.04%, well within the 17.5% maximum allowed EVM for a UMTS repeater [5].

Fig. 11(a) gives the SER performance of the ICS for various values of the SNR, assuming AWGN and Rayleigh fading channels between antennas of the ICS relay. Fig. 11(a) shows that the SER is improved when the ICS is active. The tracking ability of the ICS is plotted in Fig. 11(b). Fig. 11(b) shows that as the radio echo Doppler frequency increases, the MSE increases. This implies that the ICS relay fails to track the rapid fluctuations, as the fading level increases. Finally, Fig. 11(c) presents a plot of the step-size versus the MSE to find the optimum value of the step-size that result in the smallest MSE. The optimum value of step-size is important since the steady-state MSE and speed of convergence of the adaptive algorithm depend upon it. Fig. 11(c) shows the optimum step-size to be 0.0001. In practice, a large step-size yields fast convergence that allows the algorithm to track rapid fluctuations due to fading, at the expense of increased noise in the channel gain estimate; which affects the interference cancellation. Similarly, a small value of the step-size makes the convergence of the adaptive algorithm slow.

In section IV, we have described a multiple-tap RES architecture. MSE of a multiple-tap RES is less than the MSE of a single-tap RES in the situation when the echo-searcher gives an incorrect estimate about the echo delay, by an integer number of samples. The MSEs of three-tap and five-tap RESs are compared with that of a single-tap RES in Fig. 12, for a radio echo delay with 100 samples. Fig. 12 shows that the MSE increases on either side of the correct position of the radio echo. Fig. 12 also shows that a three-tap RES gives a better performance than a single-tap RES. Likewise, a five-tap RES works better than a three-tap RES. However, the error floor is raised with the additional taps.

TABLE I
AVERAGE PSD OF DIFFERENT SIGNALS IN ICS

Signal	Average PSD value
Transmitted signal from BS	49.13 dBm
Interference signal	40.16 dBm
Error signal	0.43 dBm
Cancellation (relative to interference)	39.73 dBc

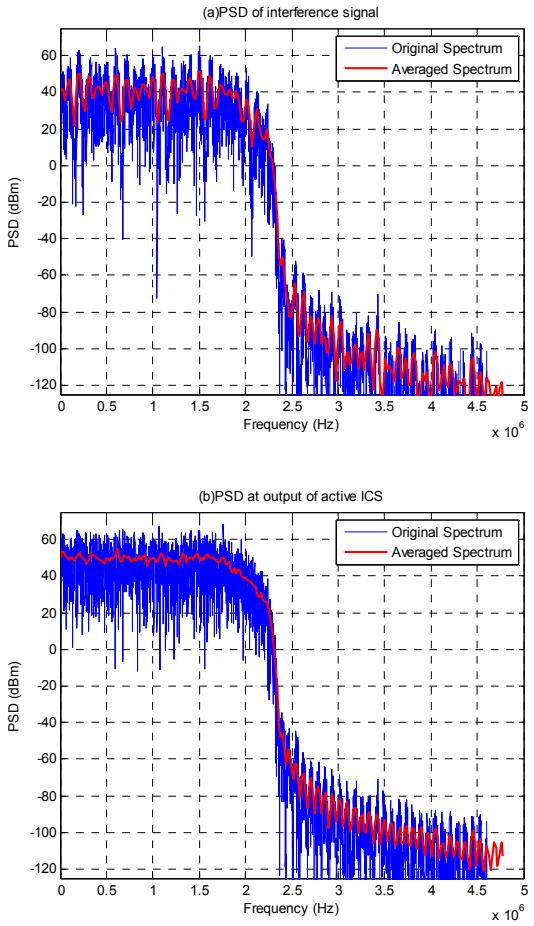

Fig. 9. Spectrum of various signals in ICS.

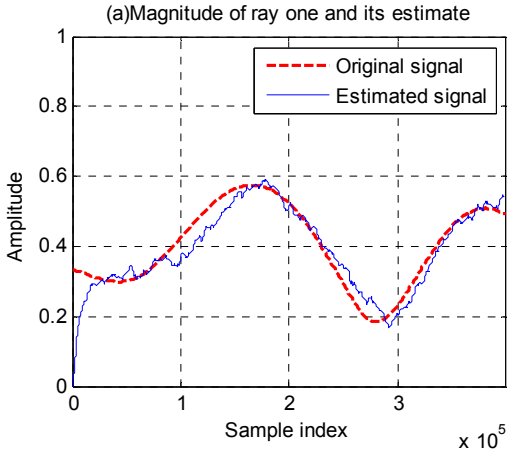

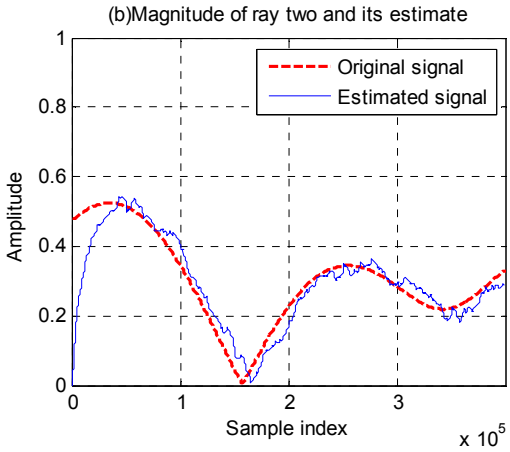

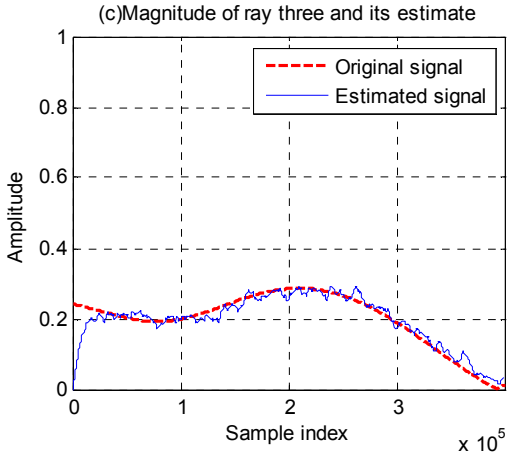

Fig. 7. Magnitude tracking ability of three radio echo suppressors.

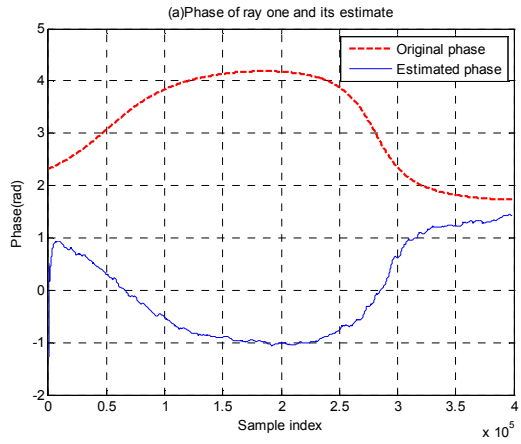

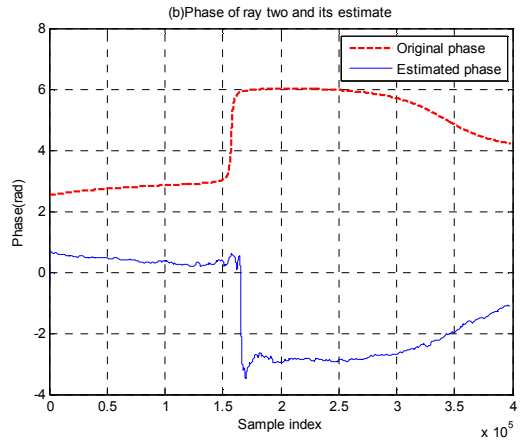

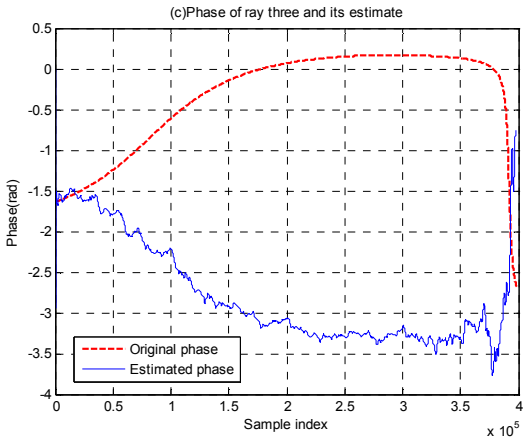

Fig. 8. Phase tracking ability of three radio echo suppressors.

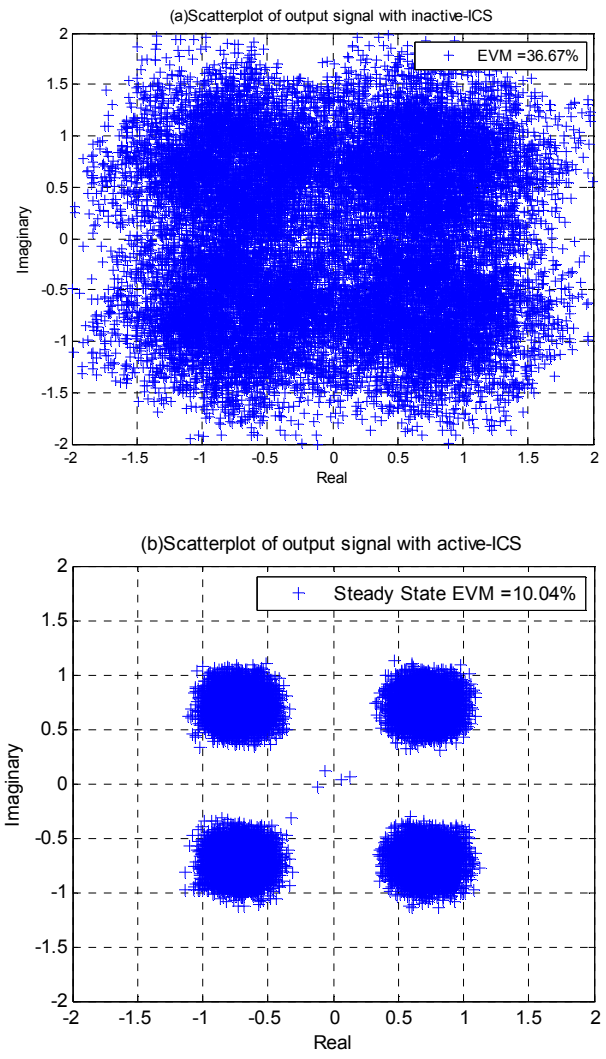

Fig. 10. Constellation plots before and after interference cancellation

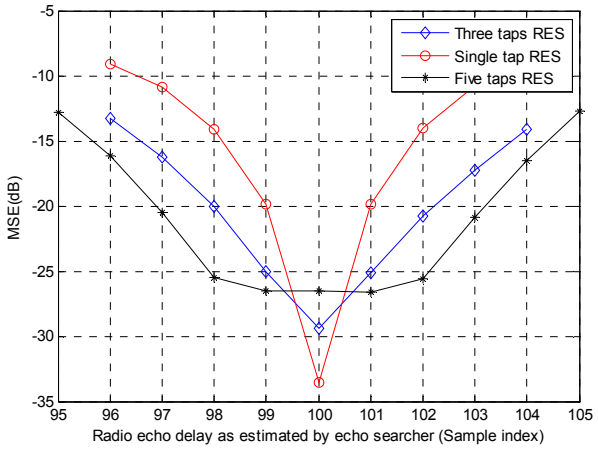

Fig. 12. MSE of multiple-taps RES.

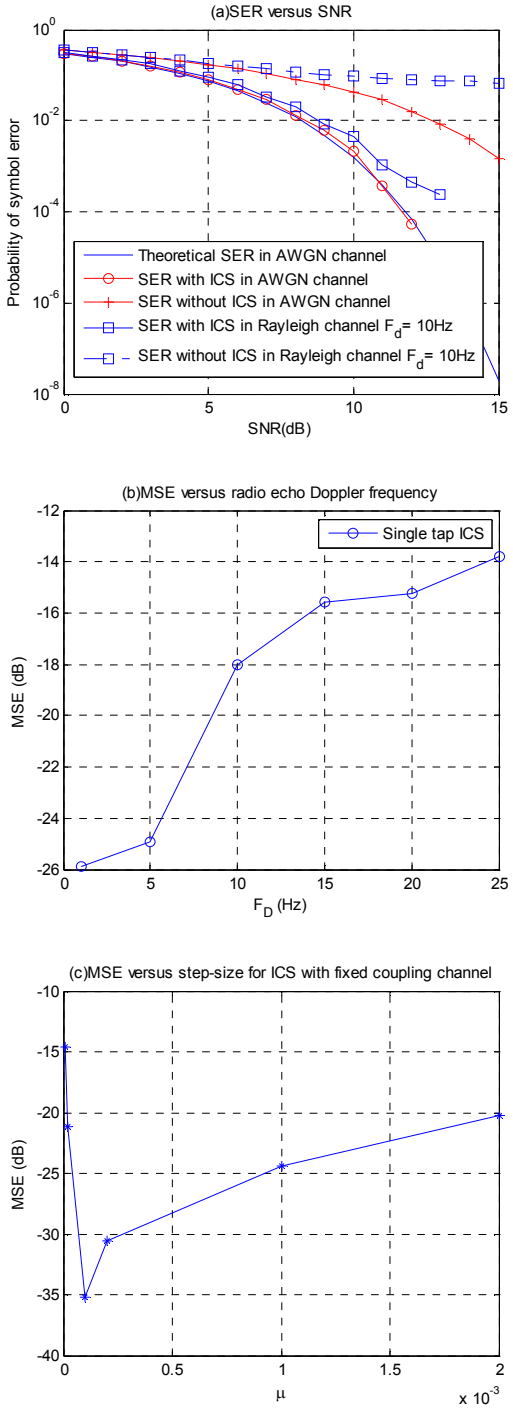

Fig. 11. Various characteristics plots of ICS.

VII. FPGA Measurement

We developed a hardware test-bed to view the real-time performance of the relay with ICS. The circuit was developed using the Xilinx System Generator and Xilinx ISE; and tested on the XtremeDSP Development Kit-IV. The suppression system was developed with a view to effectively consume the onboard resources. The data flow diagram and laboratory test bench are shown in Fig. 13 and Fig. 14 respectively. A digital down converter (DDC) and digital up converter (DUC) were also used as supplementary circuits in the test bench. A fixed tap coupling channel that is 8 dB less than the power of the

incoming signal is realized. The parameters used in the test bench are listed in Table. II. Fig. 15 gives the spectrum of modulated WCDMA signal. Fig. 16 gives the frequency response of the coupling channel. The spectrum of the error signal is given in Fig. 17. Table. III compares the FPGA and MATLAB simulation

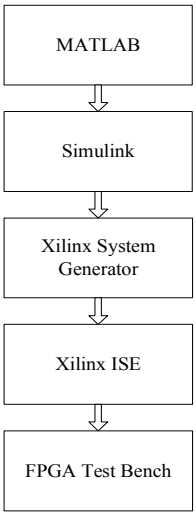

Fig. 13. Design flow of algorithm.

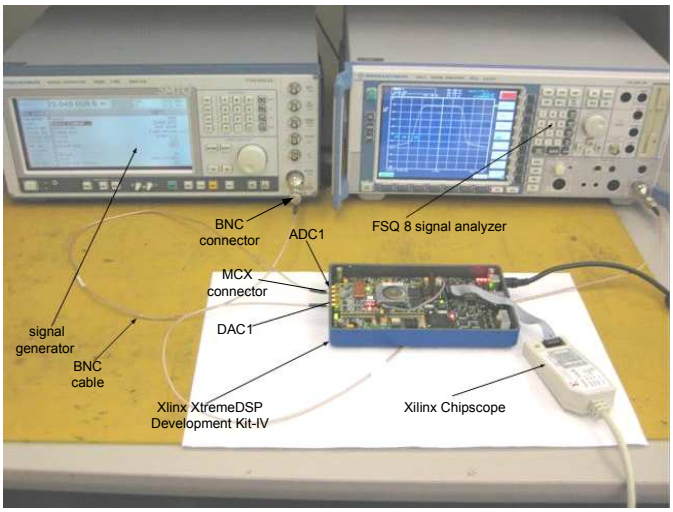

Fig. 14. Laboratory test bench.

TABLE III
COMPARISON BETWEEN MATLAB AND FPGA RESULTS

Signal	MATLAB	FPGA
Transmitted signal from BS	29.14 dBm	-12 dBm
Interference signal	13.95 dBm	-20 dBm
Error signal	0.56 dBm	-33 dBm
Cancellation relative to interference	13.39 dBc	13 dBc

TABLE II

PARAMETERS USED IN TEST BENCH

Quantity	Value	Remarks
FPGA clock frequency	92.16 MHz	onboard oscillator
WCDMA signal data rate	3.84 MSPS	WCDMA carrier
Sampling rate of WCDMA	38.4 MHz	
Bandwidth of WCDMA	5 MHz	
Number of carriers in WCDMA	1	single carrier
WCDMA carrier frequency	23.04 MHz	
Number of RES	1	
Number of radio echoes	1	
SMIQ signal level	6.2 dBm	
FSQ reference level	0 dBm	

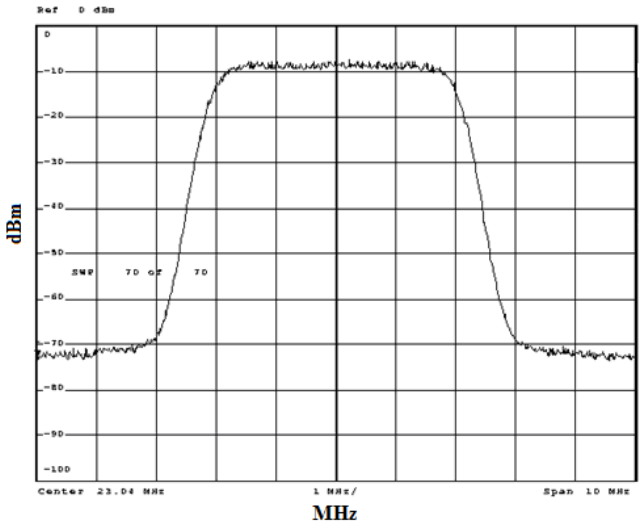

Fig. 15. Spectrum of input IF modulated WCDMA signal.

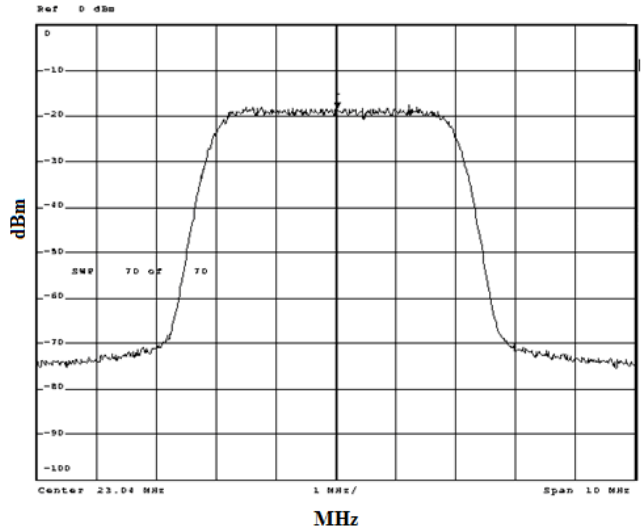

Fig. 16. Spectrum of interference signal.

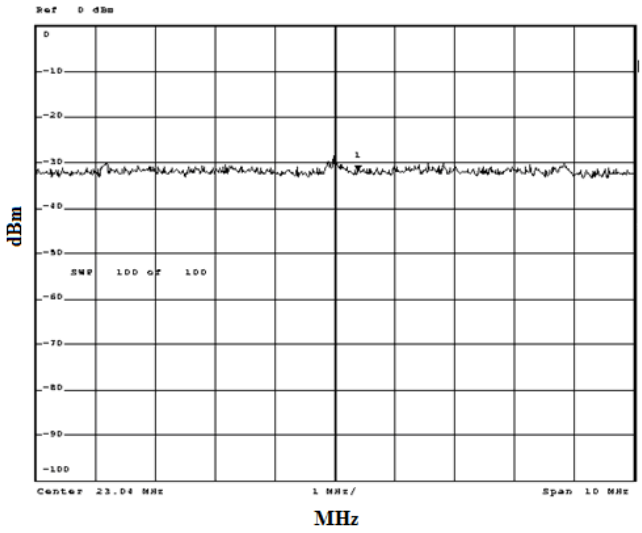

Fig. 17. Spectrum of error signal.

results. Table. 3 shows that the interference cancellation using the FPGA is 13 dB; that agrees closely with the MATLAB results. Due to the presence of quantization noise and limited floating point precision, the FPGA results can differ slightly from the MATLAB ones. These results imply that the FPGA implementation of our described algorithm is very suitable for the real-time environment. The results also conclude that Virtex-4 FPGA is a desirable processor to implement the wireless communication algorithm.

VIII. Conclusion

This paper has discussed a solution for coupling cancellation in Multi-hop 3G WCDMA wireless networks. The interference cancellation system discussed here does not require any training sequence or pilot symbols. It has far less complexity than other interference cancellation approaches. In the ICS relay, the steepest descent algorithm was used to estimate the gain of the channel. This paper has introduced a novel multi-tap RES. The multiple tap RES structure has better performance than the single tap RES when the echo delays are inaccurate. Simulation results have shown that the ICS works well with a desirable EVM. The interference cancellation ability is found to be around 40 dBc. The ICS algorithm has been verified using MATLAB simulations and a hardware test bench is developed on the XtremeDSP Virtex-4 FPGA platform. The simulated and FPGA results are compared with a high degree of agreement.

Appendix I

$$MSE_{system} = \mathbf{E}\left\{\left|\varepsilon_{system}(n)\right|^2\right\} \tag{24}$$

$$= \mathbf{E}\left\{\left|U(n)+S(n)\right|^2\right\} \tag{25}$$

$$U(n) = w_l \times C(n-D) \tag{26}$$

$$S(n) = M_l \times C(n-D) \tag{27}$$

$$\Rightarrow MSE_{system} = \sigma^2 \times \mathbf{E}\left\{\left|(w_l + M_l)\right|^2\right\} \tag{28}$$

We denote variance of the signal $C(n-D)$ by σ^2

$$\Rightarrow MSE = \frac{MSE_{system}}{\sigma^2} \tag{29}$$

$$MSE_{dB} = 10\log_{10}\left(\frac{MSE_{system}}{\sigma^2}\right) \tag{30}$$

$$= 10\log_{10}(MSE_{system}) - 10\log_{10}\left(\sigma^2\right) \tag{31}$$

$$= MSE_{system\_dB} - 10\log_{10}\left(\sigma^2\right) \tag{32}$$

Appendix II

$$\varepsilon_{system}(n) = U(n) + S(n) \tag{33}$$

$$= C(n-D)\times(w_l + M_l) \tag{34}$$

$$w = |w|e^{j\varphi_w} \tag{35}$$

$$M_l = |M_l|e^{j\varphi_{M_l}} \tag{36}$$

$$\varepsilon_{system}(n) = C(n-D)\times\left(|w|e^{j\varphi_w} + |M_l|e^{j\varphi_{M_l}}\right) \tag{37}$$

At steady-state, $|M_l| \approx |w|$ and $\varphi_{M_l} \approx |\varphi_{w_l}| \pm \pi$

$$\varepsilon_{system}(n) = C(n-D)\times\left(|w|e^{j\varphi_w} + |M_l|e^{j(\varphi_w \pm \pi)}\right) \tag{38}$$

$$= C(n-D)\times\left(|w|e^{j\varphi_w} + |M_l|e^{j\varphi_w}e^{\pm j\pi}\right) \tag{39}$$

$$= C(n-D)\times\left(|w|e^{j\varphi_w} - |M_l|e^{j\varphi_w}\right) \tag{40}$$

Appendix III

$$J_l = \mathbf{E}\left[|Q(n)|^2\right] \tag{41}$$

$$= \mathbf{E}\left[|R(n)+S(n)|^2\right] \tag{42}$$

$$= \mathbf{E}\left[|R(n)+M_l C(n-D)|^2\right] \tag{43}$$

$$= \mathbf{E}\left[|X(n)+U(n)+\zeta(n)+M_l C(n-D)|^2\right] \tag{44}$$

$$= \mathbf{E}\left[|X(n)+w_l C(n-D)+\zeta(n)+M_l C(n-D)|^2\right] \tag{45}$$

$$= \mathbf{E}\left[|X(n)+w_l C(n-D)+M_l C(n-D)|^2 + |\zeta(n)|^2\right] + \mathbf{E}\left[2|X(n)+w_l C(n-D)+M_l C(n-D)||\zeta(n)|\right] \tag{46}$$

$$= \mathbf{E}\left[|X(n)+w_l C(n-D)+M_l C(n-D)|^2 + |\zeta(n)|^2\right] + \left[2E|X(n)\zeta(n)| + \mathbf{E}|w_l C(n-D)\zeta(n)| + \mathbf{E}|M_l C(n-D)\zeta(n)|\right] \tag{47}$$

$$= \mathbf{E}\left[|X(n)+w_l C(n-D)+M_l C(n-D)|^2 + |\zeta(n)|^2\right] + \begin{bmatrix} 2\mathbf{E}|X(n)|\mathbf{E}|\zeta(n)| + w_l\mathbf{E}|C(n-D)|\mathbf{E}|\zeta(n)| \\ + M_l\mathbf{E}|C(n-D)|\mathbf{E}|\zeta(n)| \end{bmatrix} \tag{48}$$

where the signals $X(n)$ and $C(n-D)$ are assumed to be independent of $\zeta(n)$. Since it is assumed that the signal $X(n)$ and noise $\zeta(n)$ both are zero mean, than $\mathbf{E}[X(n)]=0$, $\mathbf{E}[C(n-D)]=0$ and $\mathbf{E}[\zeta(n)]=0$. Hence we are left with,

$$J_l = \mathbf{E}\left[|X(n)+w_l C(n-D)+M_l C(n-D)|^2 + |\zeta(n)|^2\right] \tag{49}$$

$$= \mathbf{E}\left[|X(n)+\{w_l+M_l\}C(n-D)|^2 + |\zeta(n)|^2\right] \tag{50}$$

ACKNOWLEDGMENT

The authors like to thank the Simon Fraser University and NSERC for their support.

REFERENCES

[1] M.R. Bavafa and H.H. Xia, "Repeaters for CDMA systems," *in Proc. IEEE VTC'98—Spring*, vol.2, pp. 1961-1965, May 1998.

[2] Jin-Yong Choi, Jin-kyu Hong, SangJin Lee, Young-Woo Suh and Jong-Soo Seo, "An interference cancellation technique for digital on-channel repeaters in T-DMB system," *in Proc. IEEE BMSB'09,* pp. 1-4,May 2009.

[3] Young-Jun Lee, Ho min Eum, Yong-Tae Lee, Kyung Sik Son and Hyoung-Nam Kim, "Performance of feedback cancellers for T-DMB on-channel repeaters," *IEEE Trans. Broadcasting,* vol.55, pp. 810-817, 2009.

[4] S.W. Kim, Y.T. Lee, S.I Park, H.M. Eum, J.H. Seo and H.M. Kim, "Equalization digital on-channel repeater in the frequency networks," *IEEE Trans. Broadcasting*, vol.52, pp. 137-146, 2006.

[5] Christopher R. Anderson, Seshagiri Krishnamoorthy, Chris G. Ranson, Todd J. Lemon, William G. Newhall, Thomas Kummetz and Jeffery H. Reed, "Antenna isolation, wideband multipath propagation measurements, and interference mitigation for on-frequency repeaters," *IEEE Proc. SECON'04,* pp. 110- 114, Oct. 2004.

[6] Hiroshi Suzuki, Kazuhito Itoh, Yoshio Ebine and Mitsuo Sato, "A booster configuration with adaptive reduction of transmitter-receiver antenna coupling for pager systems," in Proc. *IEEE VTC'99,* vol.3, pp. 1516-1520, Sept. 1999.

[7] Yong Tae Lee, Sung Ik Park, Ho Min Eum, Jae Hyun Seo, Heung Mook Kim, Seung Won Kim and Jong Soo Soe, "A design of equalization digital on-channel repeater for single frequency network ATSC system," *IEEE Trans. Broadcastin*g, vol.53, pp.23-27, 2007.

[8] Moohong Lee, Byungjik Keum, Minjae Park, Young Serk Shim, Hwang Soo Lee and Dae Ho Woo,"A frequency domain approach for complexity reduction in wideband radio interference cancellation repeaters," *in Proc. IEEE ICSP'08*, pp.1971-1976, Oct. 2008.

[9] Toshiyuki Maeyama and Takashi Inoue, "Development of cellular repeater system with radio echo suppresser," *in Proc. IEEE PIMRC'04,* vol.53, pp.23-27, Sept. 2004.

[10] Hiroyuki Hamazumi, Koichiro Imamura, Naohiko Iai, Kazuhiko Shibuya and Makoto Saski, "A study of a loop interference canceller for the relay stations in an SFN for digital terrestrial broadcasting," *in Proc. IEEE GLOBECOM'00*, vol.1, pp. 167-171, Nov. 2000.

[11] Jin-Yong Choi, Min-Sung Hur, Young-Woo Suh and Jong-Soo Seo, "A novel energy equalization digital on-channel repeater for T-DMB system in time-varying channels," *in Proc. IEEE ICCE'09,* pp.1-2, Jan. 2009.

[12] Jin-Kuk Lee, Sang-Keun Park, Heung-Jae Choi, Yong-Chae jeong and Jae-Hun Yun, "A design of co-channel feedback interference cancellation system using the analog control," *in Proc. IEEE EUMC'06*, pp. 153-156, Sept. 2006.

[13] J. G. Proakis*, Digital Communications*, 4th ed., New York: McGraw-Hill, 2000.

Saad Mahboob was born in Islamic Republic of Pakistan. He received the M.A.Sc. in Electrical Engineering from Simon Fraser University, Burnaby, Canada in 2009. He worked as a Research Assistant in Mobile Communication Lab. His research interests include OFDM, MIMO, cooperative communication and DSP applications design on FPGAs.

Shawn P. Stapleton was bom in North Bay, Ont., Canada. He received the M.Eng. degree in microwave engineering in 1984 and the Ph.D. degree in engineering in 1987, both from Carleton University, Ottawa, Canada. He is working as a Professor at Simon Fraser University in Electrical Engineering. Dr. Stapleton is a Fellow of the Advanced Systems Institute. His research at SFU has focused on integrated RF/DSP applications for Wireless Communications. While at Simon Fraser University he developed a number of Adaptive Power Amplifier Linearization techniques ranging from Feedforward, Delta-Sigma Modulators, Work Function Predistortion to Digital Baseband Predistorters. He has published over 100 technical papers on Linearization and Power Amplification and has given many international presentations on the subject.

Sami Muhaidat (S'01-M'08) received the M.Sc. in Electrical Engineering from University of Wisconsin, Milwaukee, USA in 1999, and the Ph.D. degree in Electrical Engineering from University of Waterloo, Waterloo, Ontario, in 2006. From 1997 to 1999, he worked as a Research and Teaching Assistant in the Signal Processing Group at the University of Wisconsin. From 2006 to 2008, he was a postdoctoral fellow in the Department of Electrical and Computer Engineering, University of Toronto, Canada. He is currently an Assistant Professor with the School of Engineering Science at Simon Fraser University, Burnaby, Canada. His general research interests lie in wireless communications and signal processing for communications. Specific research areas include MIMO techniques, equalization techniques, channel estimation, cooperative communications, and cognitive radio. Dr. Muhaidat is an Associate Editor for IEEE Transactions on Vehicular Technologies. He has served on the technical program committee of several IEEE conferences, including ICC and Globecom.